Turkish Journal of Electrical Engineering & Computer Sciences

http://journals.tubitak.gov.tr/elektrik/

Research Article

Turk J Elec Eng & Comp Sci
(2020) 28: 2997 – 3012

doi:10.3906/elk-1909-69

Variable gain high order sliding mode control approaches for PMSG based variable speed wind energy conversion system

Ameen ULLAH[1], **Laiq KHAN**[1,*], **Qudrat KHAN**[2], **Saghir AHMAD**[1]
[1]Department of Electrical and Computer Engineering, Faculty of Engineering, COMSATS University, Islamabad, Pakistan
[2]Center of Advance Studies in Telecommunication, COMSATS University, Islamabad, Pakistan

Received: 12.09.2019 • **Accepted/Published Online:** 08.06.2020 • **Final Version:** 25.09.2020

Abstract: This research article proposes two different variants of variable gain higher-order sliding mode control (HOSMC) strategy for a variable-speed wind energy conversion system (WECS) based on a permanent magnet synchronous generator (PMSG). The main objective is to extract the maximum wind power with reduced chattering and mechanical stress. The main flaw of the classical sliding mode control (SMC) is the high-frequency switching, called chattering, which is alleviated by employing HOSMC strategies. The control law design is based on a super-twisting algorithm (STA) and a real-twisting algorithm (RTA) with variable gains. The proposed control techniques inherit the property of robustness and successfully deal with the nonlinear behavior of the system, erratic nature of the wind speed, external disturbances as well as model uncertainties. Also, the significance of smooth control action and variable gains strongly reduce the chattering effect. For a given reference speed, the generator speed and its missing derivative are retrieved by using a uniform robust exact differentiator (URED). The performance validation and effectiveness of the proposed control techniques is supported by Matlab/Simulink simulations, carried out under varying wind speed, parametric variations, and load variations.

Key words: Super-twisting algorithm (STA), chattering, maximum power point tracking (MPPT), real-twisting algorithm (RTA), wind energy conversion system (WECS), permanent magnetic synchronous generator (PMSG), uniform robust exact differentiator (URED)

1. Introduction

The demand for electrical energy is increasing gradually and steadily around the world. The conventional energy sources are gradually depleting and resulting in environment-related problems, such as air pollution and greenhouse gases emission. To overcome these problems, the society is motivated towards research and application of alternate energy resources [1]. The efficient utilization of renewable energy sources has got much attention. Renewable energy resources are available in nature in the form of biomass, wind, geothermal, hydropower, and solar. However, among these stated different resources, wind energy is one of the most cost-competitive and a rapidly growing energy resource [2]. In the future, investment in the production of wind energy will be enhanced rapidly around the world.

In a wind electric market, many types of wind turbine systems are available. According to wind speed operation, these are classified into fixed speed (FS) WECS and variable speed WECSs. The FS-WECS operates at a fixed speed and has the advantage of being reliable and maintenance-free operation. However, due to

*Correspondence: laiqkhan@comsats.edu.pk

variations in wind speed, highly fluctuating output power is generated by the wind turbine. Besides this, the maximum power point (MPP) can be obtained at one speed only. While, the VS-WECSs can be designed to operate over a broad range of wind speeds, hence, the rotor speed can be adjusted according to the wind speed to harvest the maximum available power. Different types of electric generators have been employed in the WECSs. These include permanent magnet synchronous generators (PMSGs), doubly-fed induction generators (DFIGs), externally excited synchronous generators (EESGs) and squirrel cage induction generators (SCIGs) [3]. The PMSGs are the most commonly used machines in low power VS-WECSs due to their small size and high efficiency.

The design of MPPT algorithm and controller implementation are the two important steps in the MPPT research studies [4]. The MPPT controller forces the WECS to operate at its MPP reference to extract the maximum power from it. In other words, this control strategy maximizes the efficiency of the WECS. In literature, the most commonly used MPPT schemes are the fuzzy logic control (FLC) method, power signal feedback (PSF) technique, perturb and observe (P& O) technique, tip speed ratio (TSR) method and optimal torque control (OTC) method. These MPPT control algorithms only provide the information about the point of operation of the system for harvesting the maximum power. Consequently, WECS requires a controller to operate the system at its MPP. The controller design for WECS is another significant problem particularly for erratic nature of the wind speed. Considering the research made in the recent years about WECS, numerous control schemes have been formulated for the WECS. The classical linear proportional integral derivative (PID) controller has not been proved satisfactory due to nonlinear nature of the WECS and its wide operating speed range [5]. Some alternative methodologies have been proposed to strengthen the effectiveness of the classical PID controller. In [6], a fuzzy-logic control (FLC) is employed to obtain the coefficients of the PI scheme for improving the performance of the MPPT algorithm.

The intelligent type MPPT control paradigms, such as particle swarm optimization (PSO) [7], artificial neural network (ANN) [8] and FLC [9] have been formulated to operate the system closer to the reference value obtained through the perturb and observe (P&O), power signal feedback (PSF) or tip-speed ratio (TSR) techniques. Generally, the stated intelligent control approaches have some disadvantages, such as long training periods, large computational efforts and large memory requirement etc. In [10], the authors have proposed an adaptive control strategy for PMSG-based WECS, where the wind speed has been estimated by online training of ANN-based algorithm, and the PMSG has been adaptively controlled.

Alternately, nonlinear sliding mode control (SMC) technique performs effectively in WECS because of its robustness, simple design, disturbance rejection, insensitivity to parameter variations, reduction of order and finite-time convergence. In [11], the FLC and SMC based controllers generate the reference signal for the MPPT with variable wind speed. In [12], the authors have proposed a FLC based SMC to capture the maximum wind energy and reduce the generator-side current harmonics for a direct-driven wind power system. However, at generator side, the high switching frequency of converter results in chattering and mechanical stress due to discontinuity of control variable [13]. A high order SMC (HOSMC) scheme has been employed to maintain a constant switching frequency without loss of tracking capability and robustness [14]. In HOSMC family, the super-twisting algorithm (STA) has a simple control law that uses discontinuous time derivative to synthesize continuous control action, so that the system trajectory reaches the sliding surface within a finite-time, hence reduces the chattering effect. The classical STA prevents uncertainty and turbulence by enhancing the system state variables (system order), thus, the sliding motion is not guaranteed. In [15], implementation of a variable

gain super-twisting algorithm (VGSTA) handles this problem. Adaptive gains of the proposed algorithm were based on the known function that allowed the precise compensation of turbulence and smooth uncertainties, bounded with its derivatives. In [16], the VGSTA was designed for DFIG based WECS. Real twisting controllers avoid chattering and provides better robustness. However, the method is sensitive to unmodeled fast dynamics. To cope with the problem, recently proposed smooth second order sliding mode (SSOSM) controller also called variable gain real twisting algorithm (VGRTA) based on real twisting algorithm for relative degree 2 is a better choice[17].

The significant contributions of the work presented in this research article are as follows:

1. Variable gain HOSMC based MPPT control techniques, namely VGSTA and VGRTA is proposed for a variable speed PMSG-WECS to ensure reduced chattering, and hence the mechanical stress.

2. The application of STA driven URED retrieve the missing state (generator acceleration) to deny the use of physical sensor. The STA based soft sensor not only reduces the system cost, but also ensures robustness. Moreover, it does not depend on the initial conditions.

3. The Matlab/Simulink platform has been utilized to develop a simulation test bed for the PMSG based variable speed WECS with sensorless variable gain HOSM based MPPT control framework.

This paper is structured as follows: following the introduction section, the descriptive mathematical model of the variable speed PMSG-WECS along with input-output form of the system states is discussed in Section 2. Sections 3 and 4 present the strategy of MPPT control algorithm and the design of uniform robust exact differentiator, respectively. The proposed control techniques are designed in Section 5. Results and discussion are carried out in Section 6. Finally, Section 7 concludes the work presented in this article.

2. Mathematical modeling of the PMSG-WECS

The mathematical modeling of the PMSG-WECS is discussed in this section. The major parts of a typical PMSG-WECS include: a wind turbine mechanically coupled with a PMSG through gears, power electonic converters etc. The schematic of the overall PMSG-WECS is illustrated in Figure 1. In this paper, the wind is modeled as a random stochastic process.

2.1. Wind turbine modeling

The kinetic energy of wind is transformed into mechanical energy by the wind turbine. If this kinetic energy is fully captured by the turbine rotor, the total power would be $P_t = \frac{1}{2}\pi\rho a v_\omega^3$. In reality, the captured mechanical power, P_m is less than the total power, P_t. According to Rankine-Froude theory, the expression for wind turbine mechanical power, P_m, is

$$P_m = \frac{1}{2}\pi\rho R^2 v_\omega^3 C_p(\lambda, \beta) \tag{1}$$

where ρ represents the air mass density, R stands for the turbine blade radius, R^2 is the swept area of the turbine, v_ω represents the wind speed, C_p stands for the the power coefficient (defining the wind turbine efficiency) and λ is the tip-speed-ratio (TSR). The TSR can be defined as follows:

$$\lambda = \frac{R\Omega_h}{v_\omega} \tag{2}$$

The C_p is a nonlinear function of TSR and pitch angle (i.e. $\beta = 0$) and cannot exceed 0.593 according to Betz theory. The C_p depends on turbine characteristics and can be computed by the following expression:

$$C_p(\lambda) = 0.006\lambda - 0.0013\lambda^2 + 0.008\lambda^3 - 9.75 \times 10^{-4}\lambda^4 - 6.5 \times 10^{-5}\lambda^5 + 1.3 \times 10^{-5}\lambda^6 - 4.5 \times 10^{-7}\lambda^7 \quad (3)$$

The corresponding mechanical torque, Γ_m, is given by the following expression:

$$\Gamma_m = \frac{1}{2}\pi\rho R^3 v_\omega^2 C_\Gamma(\lambda) \quad (4)$$

The torque coefficient, C_Γ and power coefficient, C_p, are related as $C_p = \lambda C_\Gamma$.

The power coefficient, C_p, has the maximum value at λ_{opt}, as illustrated in Figure 2. Since, λ is a function of wind speed, v, therefore, λ is regulated to track λ_{opt} by controlling the rotor speed (Ω_h). Thus, it is now convenient to develop the mathematical model of the PMSG, as all the necessary details are reported. Note that the gear box (GB) is set to give a gear ratio, i, in Figure 1.

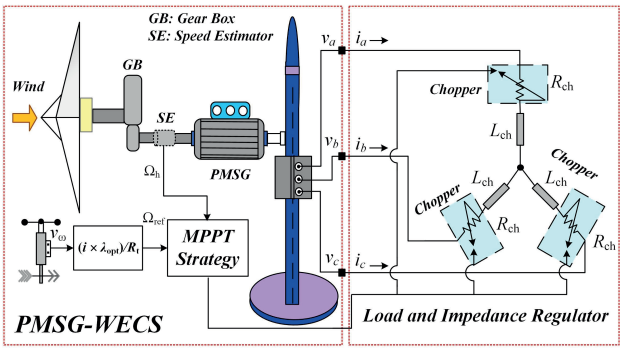

Figure 1. Overall PMSG based wind energy conversion system.

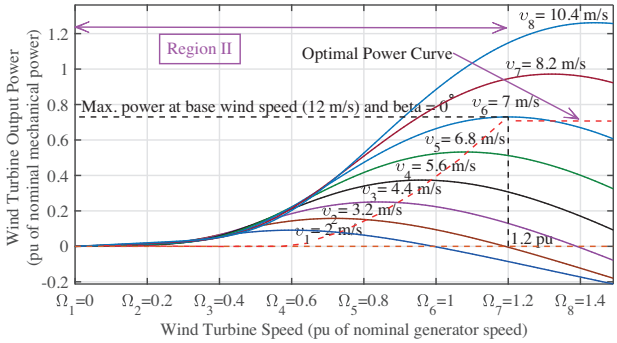

Figure 2. Turbine output power versus turbine speed for different wind speeds.

2.2. PMSG modeling

The PMSG is modeled in dq-axes frame and is given by the following set of equations [3]:

$$\frac{di_d}{dt} = -\frac{R_s + R_{ch}}{L_d + L_{ch}} i_d + \frac{p(L_q - L_{ch})}{L_d + L_{ch}} i_q \Omega_h \quad (5)$$

$$\frac{di_q}{dt} = -\frac{R_s + R_{ch}}{L_q + L_{ch}} i_q - \frac{p(L_d + L_{ch})}{L_q + L_{ch}} i_q \Omega_h + \frac{p\phi_m}{L_q + L_{ch}} \Omega_h \quad (6)$$

$$\frac{d\Omega_h}{dt} = \frac{1}{J}\left[\frac{\Gamma_w}{i} - p\Big\{(L_d - L_q) i_q i_d + \phi_m i_q\Big\}\right] \quad (7)$$

where R_s denotes the stator resistance, L_d and L_q represent the stator inductance along d and $q-axis$ of the nonsalient PMSG, respectively, (where $L_d = L_q$), L_{ch} is the load inductance, p is the number of pole pairs, ϕ_m is the maximum value of magnetic flux, i is the transmission ratio or gear ratio, J denotes the inertia

transformed to the generator side, i_d and i_q denote the stator currents along d and q-axis, respectively, Ω_h is the high speed shaft (HSS) or angular speed of the PMSG rotor and $\Gamma_w = d_1 v_\omega^2 + \frac{d_2 v}{i}\Omega_h + \frac{d_3}{i^2}\Omega_h$.

Now, let $x = [x_1, x_2, x_3]^T = [i_d, i_q, \Omega_h]^T \in \mathbb{R}^n$ be the state vector, while $u = R_{ch} \in \mathbb{R}$ stands for the control input and $y = \Omega_h \in \mathbb{R}$ represents the system output.

The nonlinear model of the system can be defined as follows:

$$\begin{cases} \dot{x} = f(x) + g(x)u \\ y = h(x) \end{cases} \tag{8}$$

with

$$\begin{cases} f(x) = \begin{bmatrix} f_1 \\ f_2 \\ f_3 \end{bmatrix} = \begin{bmatrix} a_1 x_1 + a_2 x_2 x_3 \\ b_1 x_2 + b_2 x_2 x_3 + b_3 x_3 \\ c_1 + c_2 x_3 + c_3 x_3^2 - c_4 x_2 \end{bmatrix} \\ g(x) = \begin{bmatrix} g_1 & g_2 & g_3 \end{bmatrix}^T = \begin{bmatrix} a_3 x_1 & b_4 x_2 & 0 \end{bmatrix}^T \\ h(x) = x_3 = \Omega_h \end{cases} \tag{9}$$

where $f(x) \in \mathbb{R}^n$ and $g(x) \in \mathbb{R}^n$ be the smooth vector fields, and $h(x) \in \mathbb{R}^n$ be a smooth scalar function. The constant terms in (9) are given as: $a_1 = -\frac{R_s}{L+L_{ch}}, a_2 = \frac{p(L-L_{ch})}{L+L_{ch}}, a_3 = \frac{1}{L+L_{ch}}, b_1 = -\frac{R_s}{L+L_{ch}}, b_2 = \frac{-p(L-L_{ch})}{L+L_{ch}}, b_3 = \frac{p\phi_m}{L+L_{ch}}, b_4 = \frac{1}{L+L_{ch}}, c_1 = \frac{d_1 v^2}{iJ}, c_2 = \frac{d_2 v}{i^2 J}, c_3 = \frac{d_3}{i^3 J}, c_4 = \frac{p\phi_m}{J}$.

The direct coordinates transform is expressed as follows:

$$\begin{cases} z_1 &= h(x) = x_3 \\ z_2 &= L_f h(x) = c_1 + c_2 x_3 + c_3 x_3^2 - c_4 x_3 \\ z_3 &= L_g h(x) = \frac{x_1}{x_2} \end{cases} \tag{10}$$

To achieve the input-output form of the system, the output, y, is differentiated until the input, u, appears. Hence, differentiating (10), it yields:

$$\begin{aligned} \dot{z}_1 &= z_2 \\ \dot{z}_2 &= \Big[\Big(c_2 + 2c_3 x_3\Big) f_3(x) - c_4 f_2(x)\Big] - c_4 b_4 x_2 u \\ \dot{z}_3 &= \frac{c_4}{c_1}\frac{c_1}{c_4}\left[a_1 z_3 + a_2 z_1 + a_3 z_3 u\right] - \left[\frac{c_4}{c_1}\right]^2 \left[\frac{c_1}{c_4}\right] z_3 \left[\frac{b_1 c_1}{c_4} + \frac{b_2 c_1}{c_4} z_1 + b_3 z_1 + \frac{b_4 c_1}{c_4} u\right] \end{aligned} \tag{11}$$

Since, the system relative degree, r, is one less than the system order, n, (i.e. $r < n$, where $n = 3$) and has a stable internal dynamics, z_3. Therefore, stability of z_3 has to be proved. Let $z_1 = z_2 = u = 0$ and $b_1 > a_1$, then

$$\dot{z}_3 = (a_1 - b_1) z_3$$

Consider the dynamic model of the PMSG-WECS as follows:

$$\begin{cases} \dot{z}_1 & = z_2 \\ \dot{z}_2 & = L_f^2 h(x) + L_g L_f h(x) u \\ y & = z_1 \end{cases} \tag{12}$$

where

$$\begin{cases} L_f^2 h(x) & = (c_2 + 2c_3 x_3) f_3(x) - c_4 f_2(x) \\ L_g L_f h(x) & = -c_4 b_4 x_2 \neq 0 \end{cases} \tag{13}$$

3. MPPT control algorithm

MPPT algorithm generates the reference speed corresponding to the maximum power to be captured from wind turbine at a specified wind speed. When the wind speed is below the threshold limit, the MPPT algorithm is applied. The optimal rotor speed of the PMSG at each wind speed can be derived from the following expression:

$$\Omega_{m_{opt}} = \frac{v_\omega \lambda_{opt}}{R} \tag{14}$$

The maximum mechanical power of wind turbine is computed by the following expression:

$$P_{max} = \frac{1}{2} \rho A C_{P_{max}} \frac{(R\Omega_{opt})}{\lambda_{opt}} \tag{15}$$

The maximum power, P_{max}, is obtained under varying wind speed conditions according to the rated power of WECS by regulating the turbine speed. Moreover, to operate the wind turbine system at λ_{opt}, the generator speed can also be adjusted to achieve the $C_{p_{max}}$. The P_{MPPT} is defined as a function of λ_{opt} as follows:

$$P_{MPPT} = K \lambda_{opt}^3 \tag{16}$$

$$K = \frac{1}{2} \rho A C_{p_{max}} \left(\frac{R}{\lambda_{opt}^3} \right) \tag{17}$$

where K is a constant term which specifically depends on turbine parameters and blade aerodynamics. The MPPT control algorithm is supposed to maintain the optimal speed, $\Omega_{m_{opt}}$ and optimum value of TSR (i.e. λ_{opt}) to get the maximum power from the wind turbine.

4. Design of uniform robust exact differentiator

Most of the controllers need all the state variables to implement the control algorithm. However, in practice, all the state variables are not available for measurement due to some economical and technical reasons. In order to retrieve the derivative of rotational velocity, Ω_h, an observer or differentiator is needed. A differentiator (classical) enhances the high-frequency gain. A differentiator in pure form is neither proper nor causal. Whenever a noise or spike occurs, the differentiator results in a theoretically infinite control signal, called "chaos phenomenon". So, either the differentiator is robust, but not exact, or it is exact, but not robust. The URED combines these key characteristics that results in an exact and robust output. URED is employed for the accurate estimation of the derivative of the rotational shaft speed, Ω_h, which tends to be noise free.

A URED based on super-twisting algorithm (STA) is proposed as follows:

$$\sigma = z_1 - \widehat{z}_1 \tag{18}$$

$$\dot{\widehat{z}}_1 = -\gamma_1 \phi_1(\sigma) + \widehat{z}_2 \tag{19}$$

$$\dot{\widehat{z}}_2 = -\gamma_2 \phi_2(\sigma) \tag{20}$$

Where γ_1 and γ_2 are positive constants and ϕ_1 and ϕ_2 are injecting terms which are expressed as follows:

$$\phi_1(\sigma) = |\sigma|^{\frac{1}{2}} sign(\sigma) + \xi |\sigma|^{\frac{3}{2}} sign(\sigma) \tag{21}$$

$$\phi_2(\sigma) = \frac{1}{2} sign(\sigma) + 2\xi\sigma + \frac{3}{2}\xi^2 |\sigma|^2 sign(\sigma) \tag{22}$$

where $\xi > 0$ is a scalar. When $\xi = 0$, then the standard robust exact differentiator suggested in [18] is restored. The high degree terms $|\sigma|^{\frac{3}{2}} sign(\sigma)$ and $|\sigma|^2 sign(\sigma)$ provide uniform convergence independent of the initial conditions. Moreover, $\widehat{z}_1$ and $\widehat{z}_2$ are the estimated values of Ω_h and $\dot{\Omega}_h$, respectively. Figure 3 shows the implementation of Equations (18)–(22) that develop a uniform robust exact differentiator.

5. Control system design for maximum power extraction

The conventional SMC suffers from chattering phenomenon due to the discontinuous signum function. This chattering phenomenon is alleviated by formulating the HOSMC technique. The HOSMC is a recently developed scheme, which eliminates the restrictions of conventional SMC, while maintaining its essential characteristics of robustness and finite-time convergence.

The control of shaft speed of AC generator in PMSG-WECS is a tracking problem, since it requires tracking of the desired reference speed. Consequently, tracking error, e_1 can be defined as:

$$e_1 = z_1 - z_{1ref} \tag{23}$$

The MPPT controller must be designed to derive the tracking error, e_1, to zero (i.e. $e_1 \to 0$). In SMC, the overall control law consists of an equivalent control, u_{eq}, and a switching control, u_{sw}. In this research article, the switching control law, u_{sw} is based on a variable gain STA (VGSTA) and a variable gain RTA (VGRTA).

5.1. Variable gain super-twisting algorithm

The main feature of the VGSTA is to provide 2-sliding surfaces for a relative degree one problem ($r = 1$). VGSTA does not require the information of the derivative of the sliding surface, s and removes the chattering effect caused due to a signum function in continuous manner.

The sliding surface, s, can be defined for relative degree one problem for achieving the desired goal, as follows:

$$s = \dot{e}_1 + \lambda e_1 \tag{24}$$

Since, only z_1 is available, hence its missing derivative, z_2, is estimated via the URED, as discussed in Section 4. Therefore, $\dot{z}_1$ is replaced by $\widehat{z}_2$, which is the estimated derivative of z_1. Thus,

$$s = (\widehat{z}_2 - \dot{z}_{1ref}) + \lambda(z_1 - z_{1ref}) \tag{25}$$

where λ is a positive design constant.

Taking the derivative of the sliding surface, s, in (25) as follows:

$$\dot{s} = L_f^2 h(x) + L_g L_f h(x) u - \ddot{z}_{1ref} + \lambda(\widehat{z}_2 - \dot{z}_{1ref}) \tag{26}$$

From (26), equivalent control law, u_{eq}, can be derived as follows:

$$\left.\begin{aligned} \dot{s} &= 0 \\ u_{eq} &= \frac{1}{L_g L_f h(x)} \left(\ddot{z}_{1ref} - L_f^2 h(x) - \lambda \dot{e}_1\right) \end{aligned}\right\} \tag{27}$$

The switching control law, u_{sw}, can be written as follows:

$$u_{sw} = -k_1(s,t)\psi_1(s) - \int_0^t k_2(s,t)\psi_2(s) \tag{28}$$

where

$$\psi_1(s) = k_c |s|^{\frac{1}{2}} sign(s) \qquad k_c > 0 \tag{29}$$

$$\psi_2(s) = \psi_1'(s)\psi_1(s) = \frac{1}{2} k_c^2 sign(s) \tag{30}$$

where k_c, not present in the original algorithm, is considered as an additional tuning gain to allow a better performance of the control system with respect to the chattering. Moreover, ψ_1' is the partial derivative of ψ_1 with respect to s. The variable gains are k_1 and k_2. Theses gains make the sliding surface insensitive to disturbances increasing with bounds and resulting from known functions.

For the four constants, $\epsilon > 0$, $p_1 > 0$, $p_2 < -\epsilon$ and $p_3 > 0$ verifying $p_1 p_2 > p_2^2$, the variable gains of u_{sw} can be selected as follows:

$$k_1 = \frac{p_3}{(p_1 p_3 - p_2^2)} \left[\frac{(p_3 \varrho_2 - p_2 \varrho_1)^2}{-4(p_2 + \epsilon)} + p_1 \varrho_1 - p_2 \varrho_2 - \frac{p_1 p_2}{p_3} + \epsilon \right] + \delta \qquad \delta > 0 \tag{31}$$

$$k_2 = \frac{p_1}{p_2} - \frac{p_2}{p_3} k_1 \tag{32}$$

where $\varrho_1 \geq 0$ and $\varrho_2 \geq 0$ are the known continuous functions and are expressed as follows:

$$\left.\begin{aligned} \varrho_1 &= \frac{1}{k_c} |s|^{\frac{1}{2}} (A_1 + A_2 |s| + A_3 |s|^2) \\ \varrho_2 &= \frac{A_0}{k_c^2} \end{aligned}\right\} \tag{33}$$

Finally, the overall control law under VGSTA can be expressed as follows:

$$u = \frac{1}{L_g L_f h(x)} \left[\ddot{z}_{1ref} - L_f^2 h(x) - \lambda \dot{e}_1 - k_1(s,t)\psi_1(s) - \int_0^t k_2(s,t)\psi_2(s) \right] \tag{34}$$

Theorem 1 *For some known continuous functions,* $\varrho_1(s,t) \geq 0$ *and* $\varrho_2(s,t) \geq 0$*, satisfying the inequality conditions defined in (33) and the variable gains selected according to (31) and (32), the system trajectories will reach the sliding surface,* $s = 0$*, in finite-time, irrespective of perturbation for any initial condition* [19].

5.2. Variable gain real-twisting algorithm

Variable gain RTA (VGRTA) is employed for systems with relative degree two ($r = 2$). It requires the measurement of 2^{nd} derivative of the sliding surface manifold, s, for the implementation of control law. In VGRTA, the system trajectories twist infinitely around the origin with a finite-time convergence. The VGRTA eliminates the chattering effect to provide good robustness properties as well as finite-time convergence.

The sliding surface is defined for relative degree two system as follows:

$$s = e_1 = z_1 - z_{1ref} \tag{35}$$

Taking the derivative of the sliding surface, s, in (35) as follows:

$$\left.\begin{aligned} \dot{s} &= \hat{z}_2 - \dot{z}_{1ref} \\ \ddot{s} &= L_f^2 h(x) + L_g L_f h(x).u_{eq} - \ddot{z}_{1ref} \end{aligned}\right\} \tag{36}$$

Here $\dot{z}_1$ is replaced by $\widehat{z}_2$, since it is estimated via the URED.

By putting $\dot{s} = \ddot{s} = 0$, the equivalent control law, u_{eq}, can be derived as follows:

$$u_{eq} = \frac{1}{L_g L_f h(x)}(-L_f^2 h(x) + \ddot{z}_{1ref}) \tag{37}$$

The switching control law, u_{sw}, has the following form:

$$u_{sw} = -k_1 |s|^{\frac{p-2}{p}} sign(s) - k_2 |\dot{s}|^{\frac{p-2}{p-1}} sign(\dot{s}) \tag{38}$$

where $k_1, k_2 > 0$ and $p \geq 2$ is employed.

The overall control law based on VGRTA for PMSG-WECS is given as follows:

$$u = \frac{1}{L_g L_f h(x)} \left[-L_f^2 h(x) + \ddot{z}_{1ref} - k_1 |s|^{\frac{p-2}{p}} sign(s) - k_2 |\dot{s}|^{\frac{p-2}{p-1}} sign(\dot{s}) \right] \tag{39}$$

Figure 4 shows the closed-loop system including the proposed control paradigms.

Let the variables, $s_0 = s$ and $s_1 = \dot{s}$, then the closed-loop system in state-space form can be written as follows:

$$\left.\begin{aligned} \dot{s}_0 &= s_1 \\ \dot{s}_1 &= -k_1 |s_0|^{\frac{(p-1)}{p}} sign(s_0) - k_2 |s_1|^{\frac{(p-2)}{(p-1)}} sign(s_1) \end{aligned}\right\} \tag{40}$$

Theorem 2 *The system expressed in (40) is globally and uniformly finite-time stable. In addition, the system produces a smooth second-order sliding motion only at the origin.*

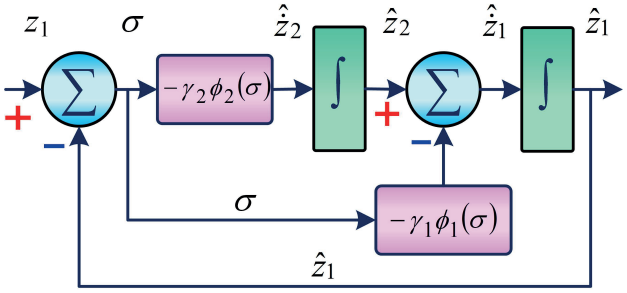

Figure 3. Uniform robust exact differentiator.

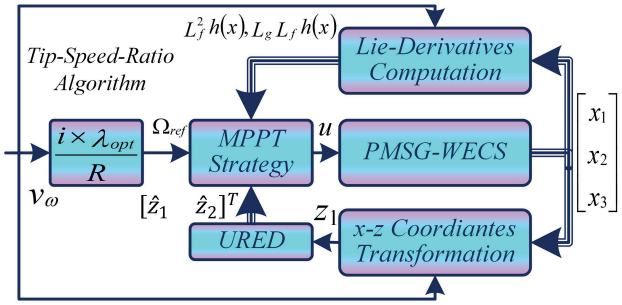

Figure 4. Closed-loop control for PMSG-WECS.

The only possible equilibrium point for the system in (40) is the origin, i.e. $s_0 = s_1 =$O(0,0). Consider a Lyapunov candidate function, $V(s_0, s_1)$, expressed as follows:

$$V(s_0, s_1) = \frac{p}{2(p-1)} k_1 |s_0|^{\frac{2(p-1)}{p}} + \frac{1}{2} s_1^2 \tag{41}$$

which is differentiable, positive definite and radially unbounded. Its derivative with respect to time is given as follows:

$$\dot{V} = k_1 |s_0|^{\frac{(p-2)}{p}} \dot{s}_0 sign(s_0) + s_1 \dot{s}_1 \tag{42}$$

It can be written as:

$$\dot{V} = k_1 |s_0|^{\frac{(p-2)}{p}} s_1 sign(s_0) - k_1 |s_0|^{\frac{(p-2)}{p}} s_1 sign(s_0) - k_2 |s_1|^{\frac{(p-2)}{(p-1)}} s_1 sign(s_1) \tag{43}$$

and, therefore,

$$\dot{V}(t, s) = -k_1 |s_1|^{\frac{(2p-3)}{(p-1)}} \tag{44}$$

Since the origin, O(0,0), is the only possible point of equilibrium for the system in (40), applying LaSalle's invariance principle for smooth systems, the only possible trajectories of (44) on the invariant manifold, $\dot{V} = 0$ as $s \equiv 0$. This indicates that the system is (i.e. asymptotically, uniformly and globally) stable with respect to the origin. The computational flowchart for implementation of the proposed control strategies is depicted in Figure 5.

6. Results and discussions

Matlab/Simulink is used to implement the entire PMSG based WECS along with the proposed nonlinear control paradigms for performance evaluation. The simulation parameters of the PMSG based WECS are listed in Table . The maximum power coefficient, $C_{p_{max}}$ of the PMSG based WECS equals 0.476 that corresponds to an optimal TSR of $\lambda_{opt} = 7$. Figure 6 shows the wind speed profile. By using a standard Von Karman spectrum, the wind speed profile is limited to a range between 4 and $9m/s$, with average speed and intensity of $7m/s$ and 0.15, respectively.

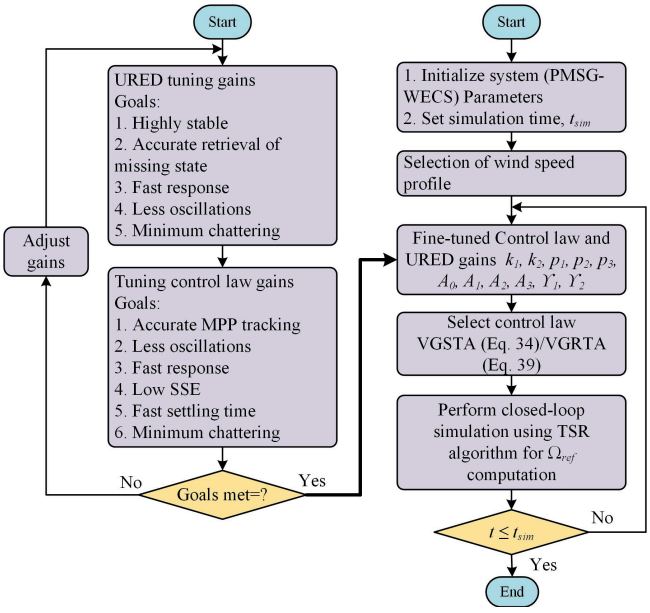

Figure 5. Computational flowchart.

Table . Different significant parameters of the PMSG based WECS.

Quantities	Symbols	Magnitude
Air density	ρ	$1.25\,\mathrm{kg\,m^{-3}}$
Radius of blades	R	2.5 m
Optimal tip speed ratio	λ_{opt}	7
Max. power coefficient	$C_{p_{max}}$	0.47
Gear ratio	i	7
Inertia	J	$0.0552\,\mathrm{kg\,m^2}$
Stator resistance	R_s	3.3 Ω
Inductance along $d-axis$	L_d	41.56 mH
Inductance along $q-axis$	L_q	41.56 mH
Pole pairs	p	3
Flux	ϕ	0.4382 Wb

The main objective of the proposed VGSTA and VGRTA based nonlinear control techniques is to maximize the power extraction from the wind under varying wind speed conditions, while maintaining the TSR at its optimal value. To evaluate the performance and robustness of the proposed control schemes, the simulation results are organized in two different cases: Case 1, test under nominal conditions; and Case 2, test under varying load and varying PMSG inertia. The results of the proposed MPPT control techniques are compared with the benchmark feedback linearization control technique (FBLC) [3].

6.1. Case 1: test under nominal conditions

The test simulations are carried out to extract the maximum power with standard parameters of the system. The wind turbine is operated at λ_{opt} and $C_{p_{max}}$ through regulating the PMSG's rotational speed at optimum values. All three candidate control techniques confirm the tracking of rotational speed, while maintaining the

TSR at its optimal value, $\lambda = 7$, and C_p at $C_{p_{max}} = 0.476$, as depicted in Figures 7–9. It is evident from the zoomed-in version of Figure 7, that the PMSG rotor speed, Ω_h, tracks the reference speed, Ω_{ref}, more closely and correctly. While comparing the reference speed tracking, the FBLC strategy shows oscillatory behavior (chattering) with a substantial steady-state error. On the other hand, the proposed VGRTA and VGSTA control paradigms show minor oscillations (chattering) as compared to the FBLC. Furthermore, the FBLC scheme tracks the generator speed, Ω_h, to the reference speed, Ω_{ref}, in around 1.507 s, while the proposed VGRTA and VGSTA control techniques track the reference speed in around 0.007 s and 6.765×10^{-5} s, respectively. Compared with the VGRTA and FBLC schemes, the VGSTA's power coefficient, C_p and TSR approach their set points accurately. Therefore, the MPPT is more effective in case of the VGSTA scheme.

Similarly, in the case of VGRTA and VGSTA, the mechanical power of the shaft around the ORC is more appealing than that of the FBLC, which confirms the reduction of chattering.

In this analysis, the generator torque against TSR and mechanical power on the generator side versus HSS speed is displayed in Figures 10 and 11, respectively. In Figure 10, the variations of mechanical torque on the generator side around ORC is smoothly tracked in case of VGRTA and VGSTA which ensure the alleviation of chattering. It is obvious from the results that the performance of VGRTA and VGSTA is far better than the performance of the FBLC. Moreover, it is apparent from the results that the performance of VGSTA is better than the performance of VGRTA in terms of operating on top of ORC, achieving $C_{P_{max}}$ and λ_{opt} with minimum chattering which guarantees the extraction of maximum power from wind.

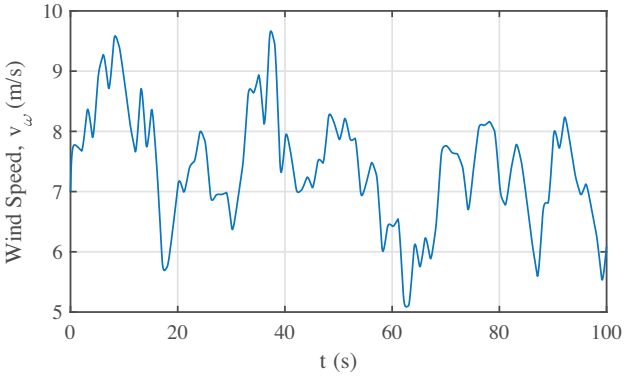

Figure 6. Wind speed profile.

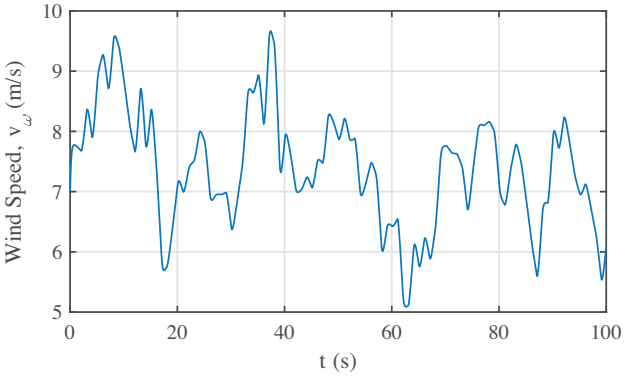

Figure 7. Evolution of PMSG rotational speed.

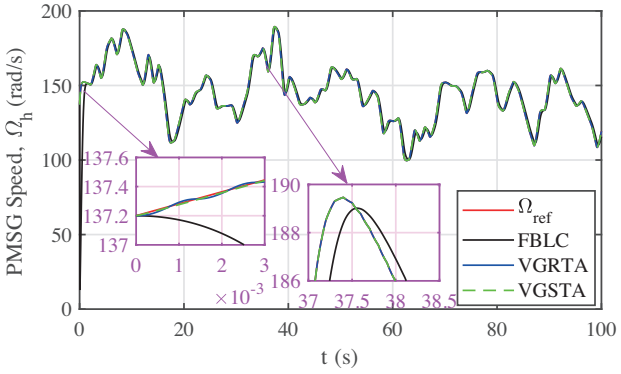

Figure 8. Comparison of power coefficient.

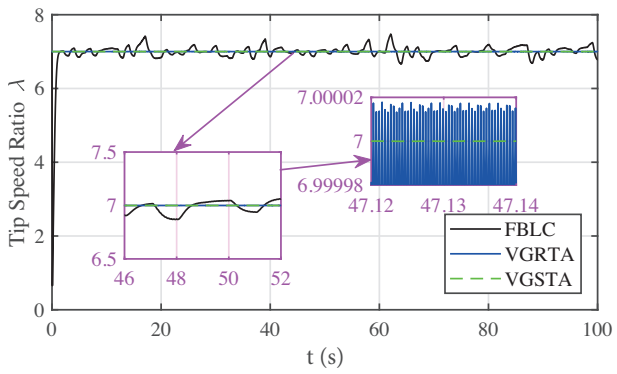

Figure 9. Evaluation of tip-speed-ratio.

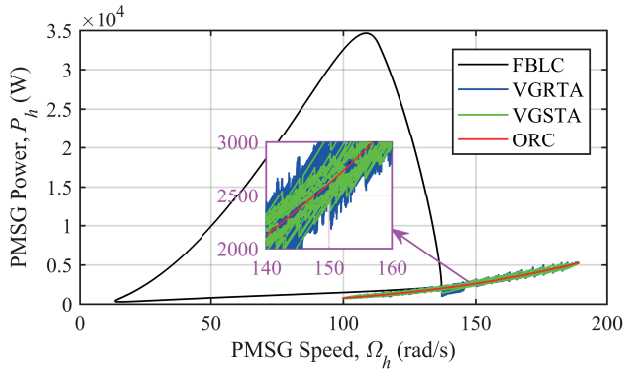

Figure 10. Optimal power point tracking on PMSG side.

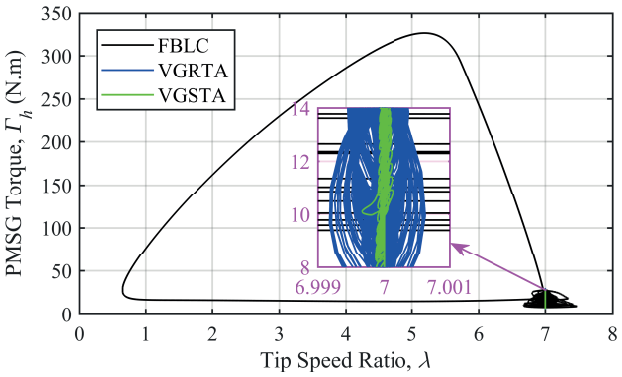

Figure 11. PMSG torque vs. tip-speed-ratio, λ.

6.2. Case 2: test under varying load and varying PMSG inertia

Once the MPPT performance of the proposed control techniques is assessed, model uncertainties are included to validate its robustness against parametric variations. The parametric variations are incorporated into the system model as follows:

- The load is varied from 0.08 to 2.085 in the time interval of (20 to 35 s).
- The PMSG inertia is varied from 0.0552 to 0.70 in the time interval of (70 to 85 s).

The variation of load and inertia are illustrated in Figure 12. Figure 13, illustrates the comparison of the PMSG speed for the three control candidates under parametric variations. The VGSTA shows better tracking of the PMSG speed, as depicted in the zoomed-in sections of the stated figure. While the FBLC and the VGRTA schemes exhibit some steady-state error and overshoots during tracking and deviate from the reference speed, which can lower the power extraction. The power coefficient, C_p and TSR of FBLC and VGRTA show some disturbance and error but no such error is observed in the case of VGSTA as illustrated in Figure 14. The VGSTA scheme maintains C_p at its optimum value, which confirms its robustness against parametric variations. The tip-speed-ratios variation with time and the PMSG power variation with its rotational speed can be seen in Figures 15 and 16, respectively. The VGSTA scheme proves itself the best candidate for maintaining the tip-speed-ratio at its optimal value, $\lambda_{opt} = 7$. Although FBLC and VGRTA schemes exhibit much larger deviations from the optimal regime characteristic (ORC), no such considerable deviation can be observed in the VGSTA strategy. From the PMSG torque vs the tip-speed-ratio evolution, depicted in Figure 17, it can be concluded that the operating point is driven much closer to the optimum value of the tip-speed-ratio, $\lambda_{opt} = 7$, by the VGSTA scheme, thus ensuring the maximum power extraction, when compared with the FBLC and VGRTA schemes. Therefore, it can easily be concluded that the proposed VGSTA and VGRTA based HOSMC strategies are much robust against load variations and insensitive to parametric variations than the feedback linearization based benchmark control strategy. Moreover, among the proposed control schemes, VGSTA outshines the VGRTA in overall performances.

7. Conclusion

The article presented two versions of the higher–order sliding mode control strategy to deal with the chattering phenomenon and the mechanical stress found in the conventional sliding mode control strategy. The proposed

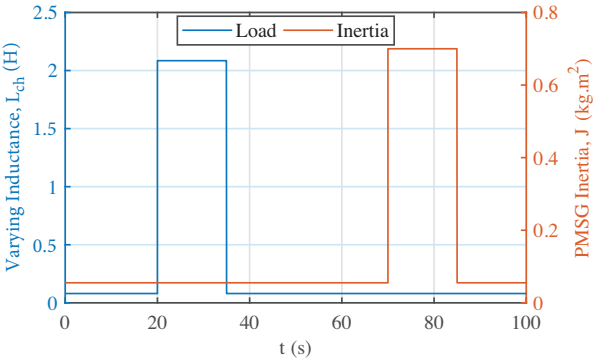

Figure 12. Variation in inertia of PMSG and load for case 2 study.

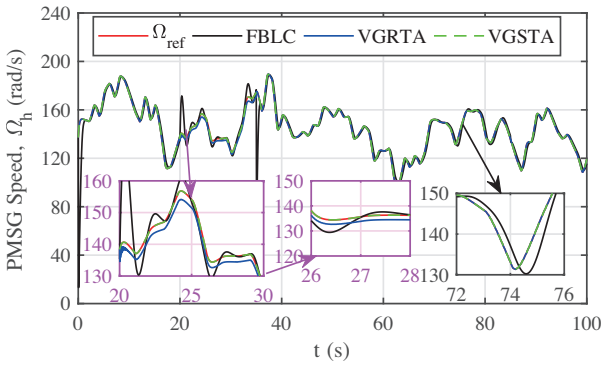

Figure 13. Evolution of PMSG speed tracking under varying load and inertia.

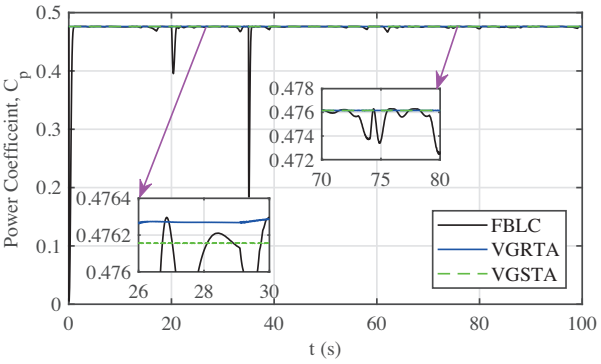

Figure 14. Comparison of power coefficients under varying load and PMSG inertia.

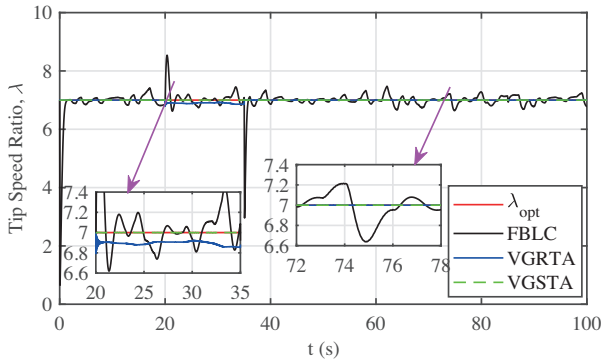

Figure 15. Tip-speed-ratio evaluation under varying load and PMSG inertia.

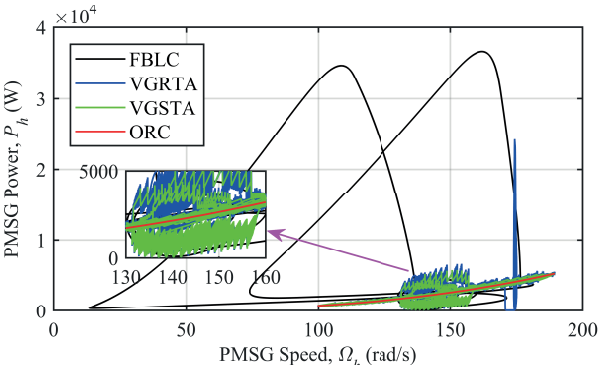

Figure 16. Optimal power point tracking under varying load and inertia.

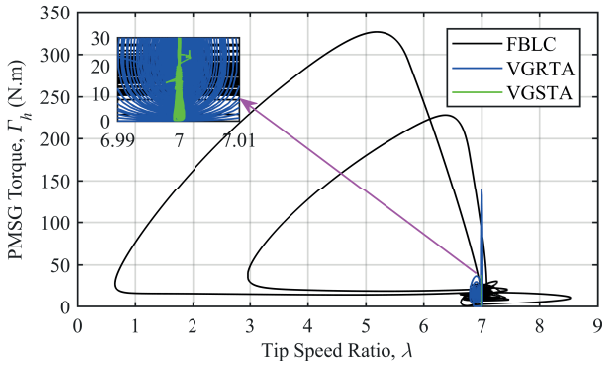

Figure 17. Generator torque vs tip-speed-ratio under varying load and inertia.

strategies, namely the VGSTA and VGRTA, have been applied to accomplish the MPPT of a variable-speed wind energy conversion system based on permanent magnet synchronous generator. The proposed control strategies inherit the properties of robustness and successfully deal with the nonlinear behavior of the system, erratic nature of the wind speed, external disturbances as well as model uncertainties. For a given reference speed, the generator speed and its missing derivative have been retrieved through a uniform robust exact

differentiator. The performance validation and effectiveness of the proposed control strategies have been supported by Matlab/Simulink simulations, carried out under varying wind speed, parametric variations, and load disturbances. The comparative analyses of simulation results revealed that both the proposed MPPT control approaches particularly VGSTA provided better performance in terms of tracking MPP (operating on ORC, achieving $C_{P_{max}}$ and λ_{opt}) with minimum chattering than the existing feedback linearizition control technique.

References

[1] Lee J, Kim YS. Sensorless fuzzy-logic-based maximum power point tracking control for a small-scale wind power generation systems with a switched-mode rectifier. IET Renewable Power Generation 2016; 10 (2): 194-202. doi: 10.1049/iet-rpg.2015.0250

[2] Hossein Y, Abbaspour A, Seraj HR. Worldwide development of wind energy and CO2 emission reduction. Environmental Energy and Economic Research 2019; 3 (1): 1-9. doi: 10.22097/EEER.2019.164295.1064

[3] Soufi Y, Kahla S, Bechouat M. Feedback linearization control based particle swarm optimization for maximum power point tracking of wind turbine equipped by PMSG connected to the grid. International Journal of Hydrogen Energy 2016; 41 (45): 20950-20955. doi: 10.1016/j.ijhydene.2016.06.010

[4] Yazici I, Yaylaci EK. Maximum power point tracking for the permanent magnet synchronous generator-based WECS by using the discrete-time integral sliding mode controller with a chattering-free reaching law. IET Power Electronics 2017; 10 (13): 1751-1758. doi: 10.1049/iet-pel.2017.0232

[5] Ganjefar S, Ghassemi AA, Ahmadi MM. Improving efficiency of two-type maximum power point tracking methods of tip-speed ratio and optimum torque in wind turbine system using a quantum neural network. Energy 2014; 67: 444-453. doi: 10.1016/j.energy.2014.02.023

[6] Ghani AA, Tahour A, Essounbouli N, Nollet F, Abid M et al. A Fuzzy-PI control to extract an optimal power from wind turbine. Energy Conversion and Management 2013; 65: 688-696. doi: 10.1016/j.enconman.2011.11.034

[7] Lin WM, Hong CM. Intelligent approach to maximum power point tracking control strategy for variable-speed wind turbine generation system. Energy 2010; 35 (6): 2440-2447. doi: 10.1016/j.energy.2010.02.033

[8] Hong CM, Ou TC, Lu KH. Development of intelligent MPPT (maximum power point tracking) control for a grid-connected hybrid power generation system. Energy 2013; 50: 270-279. doi: 10.1016/j.energy.2012.12.017

[9] Khan MJ, Mathew L. Fuzzy logic controller-based MPPT for hybrid photo-voltaic/wind/fuel cell power system. Neural Computing and Applications 2019; 31 (10): 6331-6344. doi: 10.1007/s00521-018-3456-7

[10] Jaramillo-Lopez F, Kenne G, Lamnabhi-Lagarrigue F. A novel online training neural network-based algorithm for wind speed estimation and adaptive control of PMSG wind turbine system for maximum power extraction. Renewable Energy 2016; 86: 38-48. doi: 10.1016/j.renene.2015.07.071

[11] Yin XX, Lin YG, Li W, Liu HW, Gu YJ. Fuzzy-logic sliding-mode control strategy for extracting maximum wind power. IEEE Transactions on Energy Conversion 2015; 30 (4): 1267-1278. doi: 10.1109/TEC.2015.2422211

[12] Corradini ML, Ippoliti G, Orlando G. Robust control of variable-speed wind turbines based on an aerodynamic torque observer. IEEE Transactions on Control Systems Technology 2013; 21 (4): 1199-1206. doi: 10.1109/TCST.2013.2257777

[13] Martinez MI, Tapia G, Susperregui A, Camblong H. Sliding-mode control for DFIG rotor-and grid-side converters under unbalanced and harmonically distorted grid voltage. IEEE Transactions on Energy Conversion 2012; 27 (2): 328-339. doi: 10.1109/TEC.2011.2181996

[14] Beltran B, Ahmed-Ali T, Benbouzid MEH. High-order sliding-mode control of variable-speed wind turbines. IEEE Transactions on Industrial Electronics 2009; 56 (9): 3314-3321. doi: 10.1109/TIE.2008.2006949

[15] Alejandro D, Moreno JA, Fridman L. Variable gains super-twisting algorithm: a Lyapunov based design. In: American Control Conference (ACC); Baltimore, MD, USA; 2010. pp. 968-973.

[16] Evangelista C, Valenciaga F, Puleston P. Active and reactive power control for wind turbine based on a MIMO 2-sliding mode algorithm with variable gains. IEEE Transactions on Energy Conversion 2013; 28 (3): 682-689. doi: 10.1109/TEC.2013.2272244

[17] Iqbal S, Edwards C, Bhatti AI. A smooth second-order sliding mode controller for relative degree two systems. In: 36th Annual Conference on IEEE Industrial Electronics Society (IECON); Glendale, AZ, USA; 2010. pp. 2379-2384.

[18] Cruz-Zavala E, Moreno JA, Fridman LM. Uniform robust exact differentiator. IEEE Transactions on Automatic Control 2011; 56 (11): 2727-2733. doi: 10.1109/TAC.2011.2160030

[19] Gonzalez T, Moreno JA, Fridman L. Variable gain super-twisting sliding mode control. IEEE Transactions on Automatic Control 2012; 57 (8): 2100-2105. doi: 10.1109/TAC.2011.2179878